Targeting hepatocyte growth factor receptor (Met) positive tumor cells using internalizing nanobody-decorated albumin nanoparticles

Heukers, R.; Altintas, I.; Raghoenath, S.; De Zan, E.; Pepermans, R.; Roovers, R.C.; Haselberg, R.; Hennink, W.E.; Schiffelers, R.M.; Kok, R.J.; van Bergen en Henegouwen, P.M.P.

published in
Biomaterials
2014

DOI (link to publisher)
10.1016/j.biomaterials.2013.10.001

document version
Publisher's PDF, also known as Version of record

Biomaterials 35 (2014) 601–610

Contents lists available at ScienceDirect

Biomaterials

journal homepage: www.elsevier.com/locate/biomaterials

Targeting hepatocyte growth factor receptor (Met) positive tumor cells using internalizing nanobody-decorated albumin nanoparticles

Raimond Heukers [a,1], Isil Altintas [b,1], Smiriti Raghoenath [a], Erica De Zan [b], Richard Pepermans [a], Rob C. Roovers [a,2], Rob Haselberg [c], Wim E. Hennink [b], Raymond M. Schiffelers [b,d], Robbert J. Kok [b], Paul M.P. van Bergen en Henegouwen [a,*]

[a] Cell Biology, Department of Biology, Science Faculty, Utrecht University, 3584 CH Utrecht, The Netherlands
[b] Department of Pharmaceutics, Utrecht Institute for Pharmaceutical Sciences, Utrecht University, 3584 CG Utrecht, The Netherlands
[c] Division of BioAnalytical Chemistry, AIMMS research group BioMolecular Analysis, VU University Amsterdam, 1081 HV Amsterdam, The Netherlands
[d] Laboratory Clinical Chemistry and Haematology, UMC Utrecht, 3584 CX Utrecht, The Netherlands

ARTICLE INFO

Article history:
Received 10 September 2013
Accepted 1 October 2013
Available online 16 October 2013

Keywords:
Albumin nanoparticles
Nanobody
VHH
Met
Intracellular delivery
Receptor down regulation

ABSTRACT

The hepatocyte growth factor receptor (HGFR, c-Met or Met) is a receptor tyrosine kinase that is involved in embryogenesis, tissue regeneration and wound healing. Abnormal activation of this proto-oncogene product is implicated in the development, progression and metastasis of many cancers. Current therapies directed against Met, such as ligand- or, dimerization-blocking antibodies or kinase inhibitors, reduce tumor growth but hardly eradicate the tumor. In order to improve anti-Met therapy, we have designed a drug delivery system consisting of crosslinked albumin nanoparticles decorated with newly selected anti-Met nanobodies (anti-Met-NANAPs). The anti-Met NANAPs bound specifically to and were specifically taken up by Met-expressing cells and transported to lysosomes for degradation. Treatment of tumor cells with anti-Met NANAPs also resulted in downregulation of the total Met protein. This study shows that anti-Met NANAPs offer a potential system for lysosomal delivery of drugs into Met-positive tumor cells.

1. Introduction

The hepatocyte growth factor (HGF) receptor (HGFR, c-Met or Met) is a receptor tyrosine kinase (RTK) that is primarily expressed on epithelial cells. HGF is the only known, high affinity ligand for this receptor [1]. Binding of HGF to Met activates the receptor, resulting in tyrosine phosphorylation of the receptor and the activation of several downstream signal transduction pathways such as the MAPK-, STAT- and PI3kinase/Akt-pathway [1–4]. Met/HGF signaling is important for embryogenesis and also for tissue regeneration and wound healing in the adult life [5–7]. Deregulated Met signaling is implicated in the development, progression and metastasis of a wide variety of human cancers [8,9]. This can be due to mutational activation, receptor/ligand overexpression, autocrine activation or ligand-independent activation of Met. Met is therefore an attractive target for anti-cancer therapy and several agents interfering with the Met/HGF pathway are under development such as Met/HGF signaling small molecule inhibitors, antibodies and decoy receptors [10,11]. Anti-Met therapies can be further augmented by combining them with chemotherapeutic drugs, especially when these are combined in a targeted drug delivery system [12].

Like most RTKs, ligand binding and activation of the Met tyrosine kinase initiates internalization of the receptor–ligand complexes, which is followed by intracellular trafficking and degradation of both receptor and ligand in lysosomes [11–15]. This internalization and lysosomal trafficking can be used for targeted delivery and release of drugs inside tumor cells. Previously, we designed anti-EGFR Nanobody-Albumin Nanoparticles (NANAPs), which are albumin-based nanoparticles decorated with nanobodies that target the epidermal growth factor receptor (EGFR). NANAPs were shown to bind to and internalize into EGFR-expressing cells and were found to be suitable for targeted delivery of anti-cancer drugs into cells [16].

A nanobody (or VHH) is the antigen-binding domain of heavy-chain-only antibodies found in members of the *cameilidae* family. Despite their small (~15 kDa) size, their binding affinity is similar

* Corresponding author. Cell Biology, department Biology, Science Faculty, Utrecht University, Padualaan 8, 3584CH Utrecht, The Netherlands. Tel.: +31 30 2533349; fax: +31 30 2532837.
E-mail address: p.vanbergen@uu.nl (P.M.P. van Bergen en Henegouwen).
[1] Authors contributed equally.
[2] Current address: Merus BV, Utrecht, The Netherlands.

0142-9612/$ – see front matter © 2013 Elsevier Ltd. All rights reserved.
http://dx.doi.org/10.1016/j.biomaterials.2013.10.001

to that of monoclonal antibodies [17]. Due to their small size and less complex structure nanobodies can be easily produced in prokaryotic systems giving them advantage over monoclonal antibodies or antibody fragments [18]. Nanobody-coupled liposomal and polymeric nanoparticles have already been shown to induce tumor regression in mice bearing head and neck squamous carcinoma tumors [19,20].

In this study we aimed to develop albumin nanoparticles that specifically target the Met receptor. We hypothesized that the specific uptake and lysosomal trafficking of anti-Met albumin nanoparticles would stimulate Met downregulation and allow intracellular delivery of nanoparticles into Met expressing cancer cells.

2. Materials and methods

2.1. Cell culture and cell lines

The human ovarian carcinoma cell line TOV-112D (cat nr. CRL-11731), human lung carcinoma cell line A549 (cat.nr. CCL-185) and the human epidermoid squamous carcinoma cell line A431 (cat. nr. CRL-1555) were all obtained from American Tissue Culture Collection (ATCC, LGC Standards GmbH, Wesel, Germany) and the human gastric cancer cell line MKN45 (cat. nr. ACC-409) was obtained from the Deutsche Sammlung von Mikroorganismen und Zellkulturen (DSMZ, Braunschweig, Germany). TOV-112D and A431 cells were cultured in Dulbecco's Modification of Eagle Medium (DMEM: Gibco, Invitrogen, Breda, The Netherlands) supplemented with 100 units/ml streptomycin, 0.1 mg/ml penicillin, 2 mM L-glutamine and 10% fetal calf serum (FCS) at 37°C and 5% CO_2. MKN45 cells were cultured in RPMI 1640 (Life Technologies Inc., Invitrogen) supplemented with 100 units/ml streptomycin, 0.1 mg/ml penicillin, 2 mM L-glutamine and 20% FCS. A549 cells were cultured in Ham's F12 (Life Technologies, Inc., Invitrogen) supplemented with streptomycin, penicillin, L-glutamine and 10% FCS under the previously mentioned conditions. Met expression of cells seeded for one or two days was determined by western blotting using mouse-anti-HGFR (MAB3581, R&D Systems Europe Ltd, Abingdon, UK) followed by goat-anti-mouse^{Alexa488} (Invitrogen) incubation. For the generation of the stable TOV + Met cell line, human Met-encoding cDNA (kindly provided by Dr. Morag Park, McGill University, Montreal, Canada) was first transferred from the pXM vector into a pMX-IRES-Zeo vector (generated from the pMX-SupF vector kindly provided by prof. Garry P. Nolan, Stanford University School of Medicine, Stanford, California, USA) via XhoI-XhoI digestion (Thermo Scientific, Breda, The Netherlands) and ligation (T4 ligase, Promega, Madison, USA). TOV-112D cells were transfected with this pMX-Met-IRES-Zeo using Fugene HD (Roche, Mannheim, Germany) and grown under selection pressure using 200 μg/ml of Zeocin (Invitrogen) for 8 weeks. Single clones were tested for Met-expression by western blotting.

2.2. Nanobody selection

Nanobodies directed against Met were selected using phage display technology from a phage antibody library that was made from *Llama Glama* immunized with A431 membrane vesicles, as previously described [21]. For selections, Maxisorp 96-wells plates (Nunc, Roskilde, Denmark) were coated overnight with rabbit-anti-hIgG in PBS (1:2000, Dako, Glostrup, Denmark) at 4°C. Next day, non-specific binding was blocked with 2% skimmed milk (Marvel) in PBS (MPBS) for an hour at RT. Subsequently, 1 μg of Met-Fc fusion protein diluted in MPBS (R&D systems) per well was captured for 1 h at room temperature (RT). After three washes with PBS, captured antigen was incubated with phages (blocked in 2% MPBS) for 2 h at RT. After washing, bound phages were detached by 100 mM triethylamine (TEA) elution. For phage ELISA, Maxisorp plates were coated with rabbit-anti-hIgG as described above and 50 ng/well of Met ectodomain-Fc fusion protein (R&D Systems) was captured for 1 h at RT in 2% MPBS. Single clone phages were incubated for 2 h at RT, washed extensively and bound phage was detected with mouse-anti-M13^{HRP} (1:10,000), followed by o-phenylenediamine (OPD) development. The reaction was stopped by the addition of 3M H_2SO_4 and OD was read at 450 nm. The cDNAs of the selected clones were sequenced and then re-cloned into a pET28a vector containing C-terminal Myc-6-His tags and which allows the purification of nanobodies from the periplasmic space of *E.coli*.

2.3. Production and purification of nanobodies

Nanobodies were produced as described before [16], but with minor modifications. Briefly, *E. coli BL*-21 Codon Plus (DE3)-RIL (Agilent Technologies Inc., Santa Clara, CA, USA) cells were transformed with pET28-derived nanobody-encoding plasmid and a single antibiotic-resistant colony was picked. Production was performed by growing these bacteria in 2xTY medium containing 2% (w/v) glucose and 100 μg/ml ampicillin at 37°C overnight. Four hundred milliliters of 2xTY medium (supplemented with 100 μg/ml ampicillin and 0.2% (w/v) glucose) was inoculated with the bacteria from the overnight culture with an OD_{600} of 0.1. This bacterial culture was subsequently incubated at 37 °C at 250 rpm until it reached an OD_{600} of 0.6. Subsequently, 0.5 mM IPTG was added to the bacterial culture to induce nanobody expression and the culture was further incubated at 37°C for 3.5 h. After 3.5 h, cells were spun down (5000 rpm, 15 min, 4°C) and the obtained pellet was stored over night at −20°C. The following day, periplasmic fractions were made by incubating the pellet in 6.4 ml ice cold TES (200 mM Tris–HCl, 0.5 mM EDTA, 500 mM sucrose, pH 8.0). To this suspension, 10 ml of diluted ice cold TES (1:3 in water) was added and incubated on ice for 30 min. The bacteria were spun down at 4 °C for 15 min at 5000 rpm and the supernatant was collected. The pellet was resuspended in 10 ml ice cold TES, 120 μl 1 M $MgSO_4$ was added and the mixture was incubated on ice for 30 min. The suspension was spun down at 4 °C for 15 min at 5000 rpm and the supernatant containing the nanobody was added to the previously collected supernatant. The his-tagged nanobodies were purified by means of immobilized metal ion affinity chromatography (IMAC) on TALON resin (Clontech, Palo Alto, CA, USA) according to the manufacturer's protocol (Batch/Gravity-Flow), except 50 mM NaH_2PO_4, 300 mM NaCl, 20 mM imidazole, pH 8.0 was used for all washing steps and elution was performed with the same wash buffer but containing 300 mM imidazole, pH 8.0 buffer. Imidazole was removed by means of dialysis against PBS overnight at 4°C. Finally, protein fractions and purity were analyzed by SDS polyacrylamide gel electrophoresis (SDS-PAGE). Protein concentrations were determined using a Micro BCA assay (ThermoScientific).

2.4. FACS analysis

For FACS analysis of binding of the anti-Met nanobodies, Met-expressing A431 cells were trypsinized, blocked and incubated with anti-Met VHHs (developed in house) or EGF-^{Alexa488} (Invitrogen) on ice for 2 h. The cells were washed three times with PBS and fixed in 4% paraformaldehyde (PFA). Auto-fluorescence was quenched with 100 mM glycine in PBS for 15 min and VHHs were detected with Prot-G purified rabbit-anti-VHH (developed in house), followed by goat-anti-rabbit^{Alexa488} (Invitrogen) incubation. FACS analysis was performed on a BD analyzer (BD Biosciences, Breda, The Netherlands).

2.5. Binding and affinity determination of nanobodies

TOV-112D, TOV + Met (1.5×10^4 per well) or MKN45 cells (6×10^4 per well) were seeded in a 96-wells plates (Nunc) one day before the assay. The cells were pre-incubated with binding medium (2% BSA in CO_2-independent medium (Gibco) for 10 min on ice after which the cells were incubated in binding medium supplemented with or without nanobodies (0.005–1000 nM) for 2 h on ice. After three washes with ice cold PBS, cells were fixed in 4% PFA and fixative was subsequently quenched with 100 mM glycine in PBS for 15 min. Bound nanobody was detected with rabbit-anti-VHH (1:1000) in PBS containing 2% BSA (PBA) followed by goat-anti-rabbit IRDye800CW (Li-COR Biosciences, UK, 1:500 in PBA) incubation for 1 h at RT each. Finally, cells were washed twice with PBA and fluorescence was measured using the Odyssey Infrared Imager. Binding affinity (K_D) for one site specific binding was determined by curve fitting using GraphPad Prism 5.02 for Windows (GraphPad Software, San Diego, CA).

2.6. HGF competition

HGF was labeled with ^{125}I (Perkin Elmer, USA) according to the IODO-GEN (Sigma–Aldrich) method as described previously [22]. The specific activity of I^{125}-HGF was measured at ~30,000 CPM/μg. Maxisorp 96-well ELISA plates (Nunc) were coated with rabbit anti-human IgG (Dako, Glostrup, Denmark; 4 μg/mL in PBS). The next day, wells were washed with PBS, blocked with 1% MPBS and subsequently incubated with 0.1 μg/mL of Met-ECD-Fc. After washing with PBS, the wells were incubated with 1 nM of ^{125}I-HGF in the presence or absence of 1000 nM of nanobodies for 1 h. Wells were washed four times with PBS and bound I^{125}-HGF was collected after 5 min incubation with 1 M NaOH; radioactivity was measured using a gamma counter (Wallac Wizard, Perkin Elmer). Results were analyzed using GraphPad Prism version 5.02 for Windows, GraphPad Software (San Diego, CA).

2.7. Preparation of albumin nanoparticles

Nanoparticles were prepared by the ethanolic desolvation technique as described previously [16,23] with minor modifications. Briefly, human serum albumin (HSA, 50 mg/ml) was dissolved in deionized water after which the pH was adjusted to 8.3 by addition of 0.1 M NaOH and the solution was filtered through a 0.2 μm filter (Minisart® syringe filters, Sartorius-stedim, Germany). Nanoparticles were formed by adding 92% ethanol drop wise under constant stirring. The formed particles were crosslinked with 8% glutaraldehyde (GA) overnight at RT. The nanoparticles were purified by centrifugation first at 1000 g for 5 min (pellet discarded, supernatant collected) and three times at 45,000 g for 1 h at 4°C in deionized water. Nanoparticles were stored in deionized water at 4°C. Nanoparticle yield was determined by measuring the dry weight by thermogravimetric analysis. The absence of soluble albumin and multimers was checked by SDS-PAGE (4–12% crosslinked, Invitrogen) under reducing conditions followed by Coomassie blue staining. For enabling detection of nanoparticles in fluorescence microscopy or quantification on the Odyssey Infrared Imager, nanoparticles were labeled with either Alexa488-NHS (Invitrogen) or IRDye800CW-NHS (Li-COR) as described before [16].

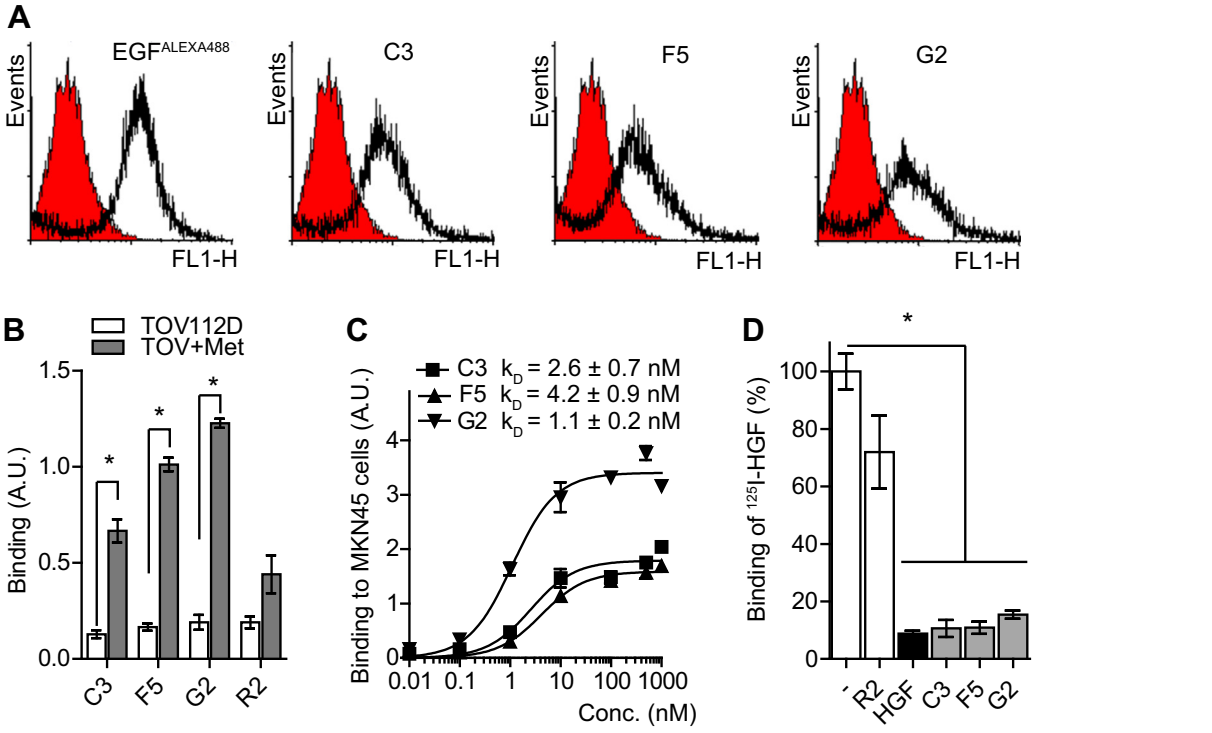

Fig. 1. The three selected anti-Met nanobodies bind Met with low nM affinities on cells. A) Binding of anti-Met nanobody C3, F5 and G2 to A431 cells measured by FACS and compared to untreated cells (red). EGF-Alexa488 was used as a positive control for binding. B) Specific binding of C3, F5 and G2 to TOV + MET cells. R2 (non-relevant nanobody) was used as a negative control. C) Binding curves and affinities (K_D) of C3, F5 and G2 on high Met-expressing cell line MKN45. D) Binding competition of ^{125}I-labeled HGF by anti-Met nanobodies. Maxisorp plates were coated with Met ectodomain and binding of 1 nM of ^{125}I-labeled HGF in the presence or absence of 1000 nM of nanobodies. Error bars represent SEM, where $n > 4$. * indicates $p < 0.001$ as determined by *t*-test.

2.8. PEGylation and G2 coupling to albumin nanoparticles

The anti-Met nanobody G2 was modified with either a 2-,4- or 8-fold molar excess of N-succinimidyl-S-acetylthioacetate (SATA) (Pierce Biotechnology, Rockford, IL, USA) as described in Ref. [19]. Briefly, the introduced sulfhydryl groups were deacetylated for 30 min at RT prior to addition of SATA-G2 to freshly prepared maleimidiyl-PEG nanoparticles. 18 mg of nanoparticles (4 mg/ml) were reacted with 14 mg of NHS-PEG3500-maleimide (15:1, mol/mol, PEG:HSA) in 0.1 M phosphate buffer (PB), pH 8 for 1 h at RT on a roller bench. PEGylated nanoparticles were collected by centrifugation and resuspended in 0.1 M PB, pH 7 and immediately reacted with SATA-modified G2 (0.1 mg G2/mg nanoparticle, 0.4 nmol G2/nmol albumin) for 2 h at RT. G2-PEG-NP were characterized for G2 coupling with dot-blot immunodetection of G2 [16].

2.9. Characterization of nanoparticles

Size distribution and polydispersity of the nanoparticles were determined by dynamic light scattering (DLS) on a Malvern ALV CGS-3 (Malvern Instruments, Malvern, UK) containing a He\Ne laser source ($\lambda = 632.8$ nm, 22 mW output power) under an angle of 90°. The zeta potential of the nanoparticles was determined using a Malvern zetasizer Nano-Z (Malvern Instruments, Malvern, UK). The measurements were performed in 5 mM PB, pH 7.4 at 25 °C.

2.10. G2-SATA characterization by capillary electrophoresis

The degree of SATA labeling on G2 was measured by means of capillary electrophoresis (CE) experiments which were carried out on a P/ACE MDQ™ CE instrument (Beckman Coulter, Brea, CA, USA). The separation voltage was −30 kV and the capillary temperature was 20 °C. Fused-silica capillaries (total length, 85 cm; inner diameter, 50 μm, outer diameter, 360 μm) were obtained from Polymicro (Phoenix, AZ, USA). The capillaries were coated with a triple layer Polybrene-dextran sulfate-Polybrene (PB-DS-PB) coating as described previously [24–26]. The background electrolyte (BGE) was 100 mM acetic acid (pH 2.8). Nanobody was hydrodynamically injected for 14 s at 1 psi (equal to 1% of the capillary volume). MS detection was performed using a micrOTOF-Q orthogonal-accelerated time-of-flight (TOF) mass spectrometer (Bruker Daltonics, Bremen, Germany). Transfer parameters were optimized by direct infusion of an electrospray ionization (ESI) tuning mix (Agilent Technologies, Waldbronn, Germany). CE-MS coupling was realized by a coaxial sheath liquid interface (Agilent Technologies, Waldbronn, Germany). A sheath liquid of isopropanol-BGE (75/25, v/v) at a flow rate of 3 μL/min was used. The following optimized spray conditions were used: dry gas temperature, 180°C; nitrogen flow, 4 L/min; and nebulizer pressure, 0.4 bar. Electrospray in positive ionization mode was achieved using an ESI voltage of −4.5 kV. CE-MS data were analyzed using Bruker Daltonics DataAnalysis software. For the determination of peak areas, extracted-ion electropherograms (EIEs) were constructed for the respective protein species from their most abundant *m/z* signals ($[M + nH]^{n+}$; $n = 12–15$). Protein charge assignment and molecular weight determinations were performed using the 'charge deconvolution' utility of the DataAnalysis software.

2.11. Cellular binding and internalization of nanoparticles

To test the binding of the NANAP's to Met-expressing cells, TOV-112D, TOV + Met, A549 (20.000 cells/well) and MKN45 (60.000 cells/well) were seed into 96-wells plates (Nunc), one day before the assay. Cells were pre-incubated with binding medium for 10 min on ice and subsequently incubated with IRDye800-labeled nanoparticles (0.06–0.5 mg/ml) for 2 h on ice. Cells were washed for 10 min with 2% Marvel in binding medium, followed by PBS, after which binding of nanoparticles was quantified with the Odyssey Infrared Imager.

For fluorescence microscopy imaging, the cells were seeded in chamber slide (Lab-Tek, Nunc) one day before the experiment. Cells were incubated with 0.25 mg/ml of Alexa488-conjugated nanoparticles in binding medium for 2 h on ice. For internalization, the nanoparticles were allowed to internalize for 2 h at 37°C. Cells were washed with binding medium and PBS extensively and fixed in 4% PFA. PFA-induced autofluorescence was quenched by incubation with 100 mM glycine in PBS for 15 min at RT and slides were mounted using SlowFade (Invitrogen). Fluorescent pictures were taken using a Zeiss LSM700 confocal microscope (Carl Zeiss Microscopy GmbH, Germany) equipped with and 63× oil immersion objective (NA 1.4).

2.12. Nanoparticle lysosomal degradation assay

Lysosomal processing of nanoparticles was studied with IRdye800-labeled nanoparticles as described previously [16]. Cells were seeded (200.000 cells/well for A549 and 600.000 cells/well for MKN45) in 12-well plates (Becton & Dickinson, Mountain View, CA, USA) one day before the experiment. Cells were pulsed with 0.25 mg/ml IRDye800-labeled nanoparticles for 2 h at 37°C. The medium was replaced by fresh medium supplemented with or without 10 μM of chloroquine (CQ, an inhibitor of lysosomal degradation, Sigma Aldrich) or lactacystin (LC, an inhibitor of proteasomal degradation, kindly provided by Dr. Marcel A.G. van der Heijden, Division of Heart and Lungs, UMC Utrecht, The Netherlands) and cells were

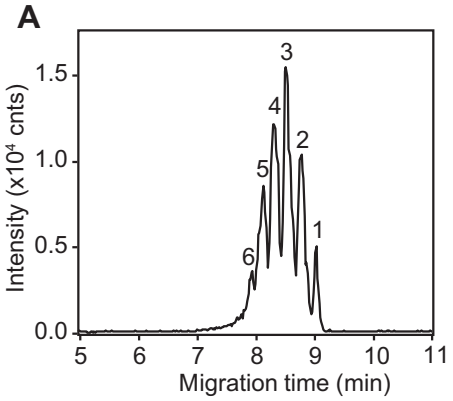

Peak no.	M_W	Rel. peak area (%)	Identity
1	17618	5.4	G2
2	17733	18.8	+1 SATA
3	17850	30.1	+2 SATA
4	17966	28.9	+3 SATA
5	18083	13.5	+4 SATA
6	18198	3.3	+5 SATA

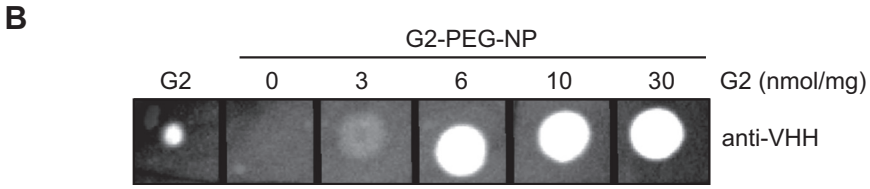

Fig. 2. Generating anti-Met NANAPs using G2. A) G2-SATA (1:8 ratio) characterization by CE-TOF-MS. B) Dot-blot analysis of G2 coupled to PEGylated nanoparticles.

incubated for an additional 16 h at 37 °C. Cells were washed with PBS and lysed in 30 μl of reducing sample buffer (50 mM Tris–HCl, pH 6.8, 10% glycerol, 100 mM DTT, 2% SDS and 0.01% bromophenol blue). IRDye800 peptide fragments were separated by SDS-PAGE and quantified using the Odyssey Infrared Imager. Mean and SEM of the intensity of the peptide bands obtained from three independent experiments were calculated.

2.13. Phosphorylation and downregulation of Met

Agonistic or antagonistic properties of G2 (1 nM, 1 μM), PEG-NP (0.5 mg/ml) and G2-PEG-NP (0.5 mg/ml) were studied using A549 and MKN45 cells that were seeded in 12 well plates (240.000 cells/well) and incubated overnight in 0.1% FBS. Formulations were diluted in 0.1% FBS medium and incubated with the cells for 30 min at 4°C. Subsequently, 50 ng/ml HGF (R&D system) was added and the cells were incubated for 10 min at 37°C. Cells were washed with PBS two times, lysed with RIPA buffer (Teknova) supplemented with Halt™ Protease & Phosphatase Inhibitor Cocktail (Thermo Scientific) and lysates were collected. For Met downregulation experiments, A549 and MKN45 cells (200.000 and 400.000 cells/well) were seeded in 24 well plates and adhered overnight, followed by incubation with 100 nM G2, 0.5 mg/ml PEG-NP or G2-PEG-NP in (serum-containing) medium for 48 h at 37°C. Next, cells were washed with PBS two times and lysed. The collected fractions were centrifuged at 15 000 g for 15 min at 4°C and the supernatant was collected and stored at 4°C. Quantification of total protein content was performed using a Micro BCA Kit (Thermo Scientific) and a fraction corresponding to 5 μg protein was loaded on a reducing SDS-PAGE gel (4–12% crosslinked, Invitrogen). Western Blot analysis was performed as previously described [16]. Total and phosphorylated Met were detected by immunoblotting with rabbit anti-phospho-Met (pY1234/pY1235) and anti-Met antibody (Cell Signaling, 1:1000 diluted) in 5% BSA-TBS-T for 2 h on the roller bench at RT. Beta-actin rabbit antibody (Cell Signaling, 1:1000 diluted) was used as a loading control. Anti-rabbit IgG HRP-linked (Cell Signalling, 1:3000 diluted) secondary antibody was added to the membrane and proteins were visualized by chemoluminescence.

2.14. Scratch wound assay

The effect of G2 and G2-PEG-NP on cell migration was assessed by a scratch wound assay as described by Liang et al. with minor modifications [27]. Briefly, cells were seeded in a 48 wells plates and allowed to adhere overnight (120.000 cells/well for MKN45 and 45.000 cells/well for A549). The following day, cells were starved in 0.1% FBS medium for 2 h and a vertical, uninterrupted wound was created in the cell monolayer using a sterile 200 μl pipette tip. Formulations were diluted in 0.1% FBS medium and incubated for 24 h. Images of the wounded cell monolayer were taken using a Nikon Eclipse Te-2000-U microscope (40× magnification) at the start of the incubations and again after 24 h. The surface of the scratch area (A) was measured using ImageJ software. Results are expressed as percentages of wound closure for each well using the formula: $100 \times [1 - (A_{t24}/A_{t0})]$. Statistical analysis was performed with GraphPad Prism software using a one-way analysis of variance (ANOVA) followed by Student's *t*-test.

3. Results

3.1. Selection and characterization of anti-Met nanobodies

To obtain nanobodies against the extracellular domain of Met, selections were performed from an in-house prepared phage nanobody library that was constructed using the immunoglobulin repertoire of peripheral blood lymphocytes of Llama immunized with vesicles from Met-expressing A431 cells [21]. After a single round of selection on the Met ectodomain, followed by a non-specific elution, binding of Met-specific clones to the Met ectodomain was tested by phage-ELISA. Of all phages that bound Met, three clones with different CDR sequences were selected (C3, F5 and G2) and these were re-cloned into a bacterial production vector. Binding of these anti-Met nanobodies to Met-expressing cells was first tested on A431 cells by fluorescence activated cell sorting (FACS) analysis (Fig. 1A). As compared to the untreated cells (indicated in red), all three nanobodies showed significant binding to A431 cells. Because A431 cells also express high numbers of EGFR, EGF-Alexa488 was taken as a control for binding. HGF was not a proper control for specific receptor binding, since this growth factor also interacts with heparin sulfates, which are present in the plasma membrane of these A431 cells [28].

To test the specificity of the nanobodies towards Met, we used Met-positive and Met-negative cell lines. The expression of Met on TOV-112D cells was first tested and these cells were confirmed to be Met-negative (Fig. S1A). Subsequently, a clone stably expressing Met was obtained by transient transfection and selection for antibiotic resistance. Stable Met-expression of different clones was determined by immunofluorescence and the cell line showing highest Met expression was selected as the Met-positive cell line, indicated as TOV + Met (Fig. S1B). All three anti-Met nanobodies showed significant binding to only the TOV + Met cells, but not to TOV-112D cells, indicating specificity towards the human Met receptor (Fig. 1B). The control nanobody R2 (directed at the Azo Dye RR6 [29]) did not significantly bind to either cell line. Subsequently, binding of the nanobodies to Met was further characterized by determining their affinity (K_D) on MKN45 cells, which overexpress Met on their

Table 1
Characteristics of albumin nanoparticles.

Nanoparticles	Size (nm)	Zeta potential (mV)	PDI[a]
NP	87 ± 9	−30 ± 3	0.06 ± 0.02
PEG-NP	106 ± 5	−18 ± 2	0.10 ± 0.03
G2-PEG-NP[b]	102 ± 3	−19 ± 4	0.10 ± 0.02

[a] Polydispersity index.
[b] 6 nmol G2/mg NP.

cell surface (Fig. 1C). All three nanobodies bound to MKN45 cells with low nanomolar affinities (2.6 ± 0.7 nM for C3, 4.2 ± 0.9 nM for F5 and 1.1 ± 0.2 nM for G2). To test whether the obtained nanobodies competed for ligand binding, an HGF competition assay was performed. As a control, an excess of unlabeled HGF was able to almost completely compete off the binding of ^{125}I-labeled HGF from coated Met ectodomain (Fig. 1D). Similarly, all three anti-Met nanobodies clearly showed competition with the labeled HGF, while the non-relevant nanobody R2 did not show any effect.

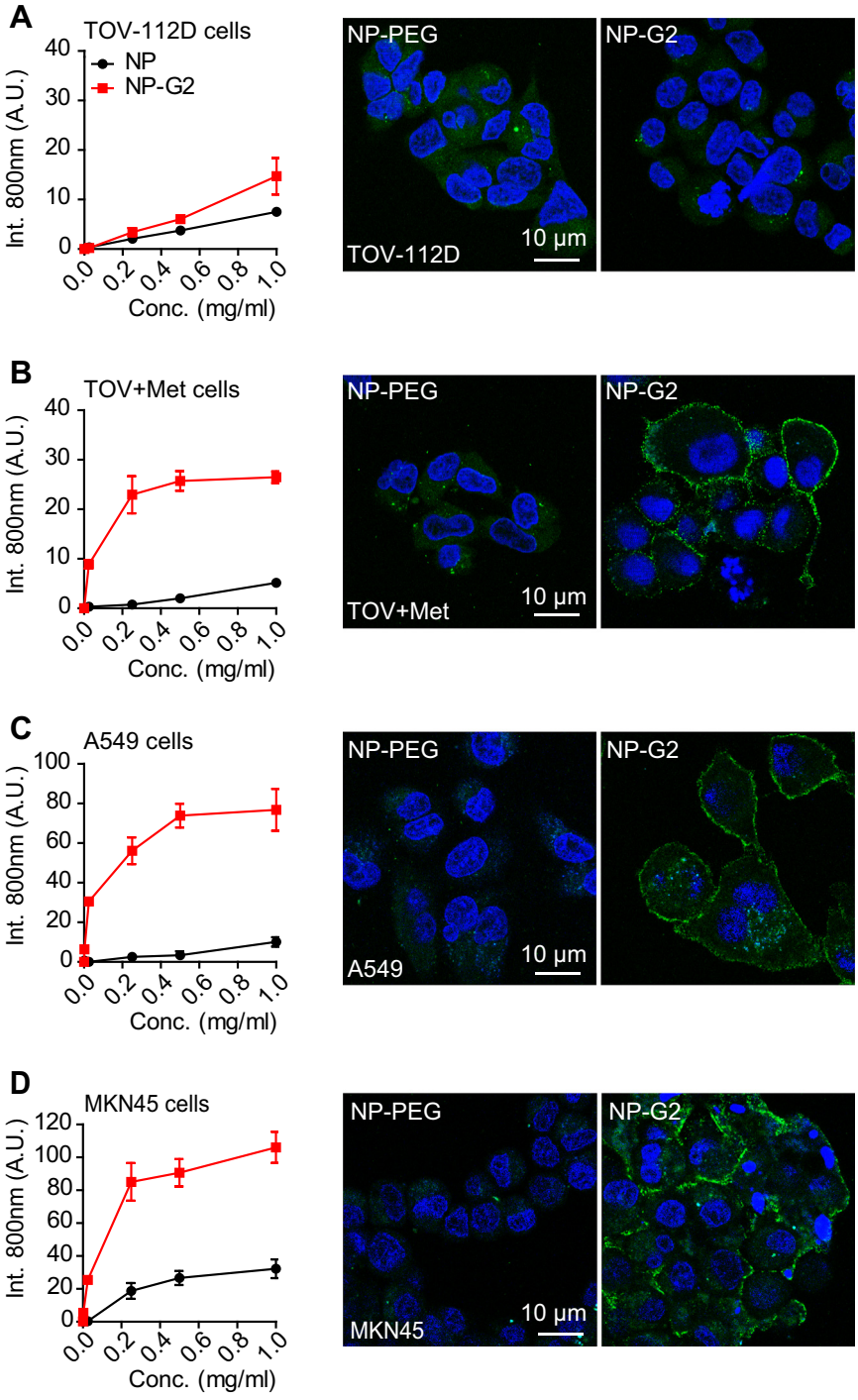

Fig. 3. G2-PEG-NPs bind specifically to Met-expressing cells. A) TOV-112D, B) TOV + Met, C) A549, or D) MKN45 cells were incubated with fluorescently labeled PEG-NP or G2-PEG-NP. A concentration range of IRDye800-conjugated NANAPs were used for determining level of binding by the Odyssey Infrared Scanner (left) and 0.5 mg/ml of Alexa488-conjugated NANAPs were used for detection by confocal fluorescence microscopy (right, indicated in green). Nuclei were stained with DAPI (blue). Error bars represent SEM, where $n = 3$.

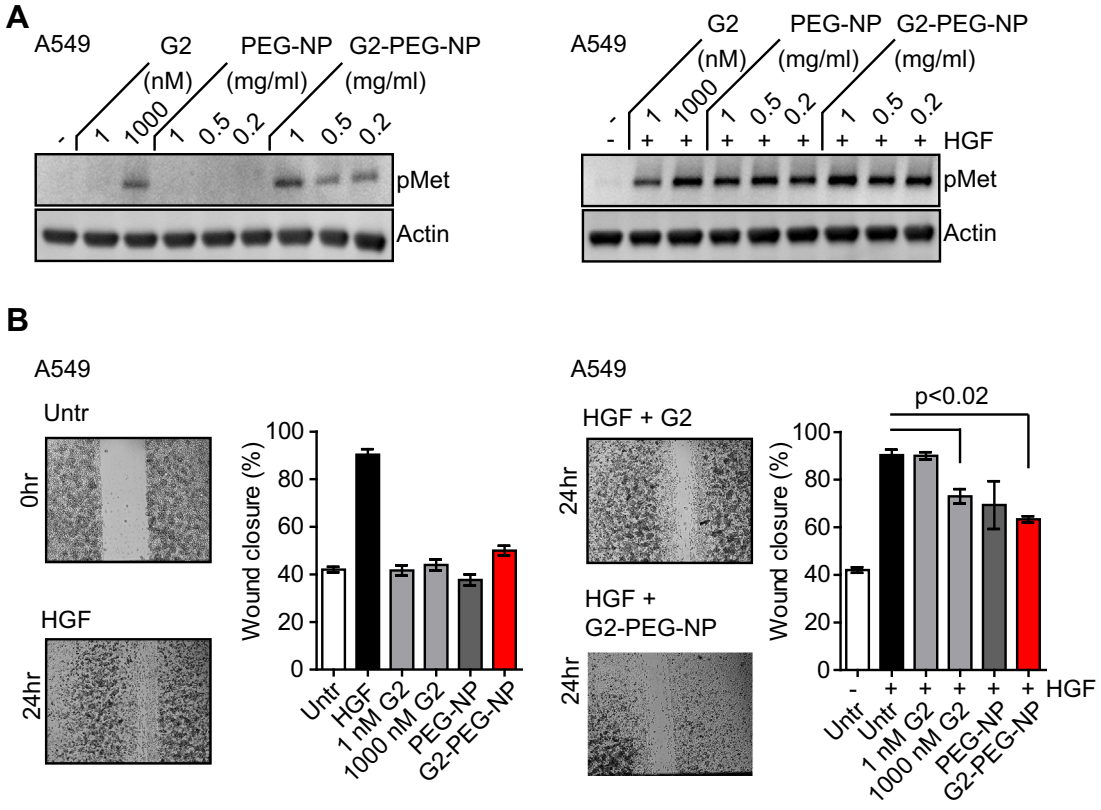

Fig. 4. Agonistic and/or antagonistic activities of nanoparticles. A, left) Activation of Met expressed in A549 cells is assessed by western blotting using anti-phospho-Met. Actin is used as a loading control. Both G2 (only at 1000 nM) and the G2-PEG-NP activate Met. A, right) Both G2 and G2-PEG-NP do not block HGF-induced Met phosphorylation. B) Scratch-wound assay in the absence (left) and presence (right) of HGF on A549 cells. None of the formulations tested induced a closure of the wound. Only G2-PEG-NP slightly reduces wound closure. Error bars represent SEM, where $n = 3$.

3.2. Modification of anti-Met nanobodies

In order to obtain nanoparticles targeting Met-expressing tumors, we decorated these particles with the selected nanobodies. This coupling was achieved via SATA groups on lysine residues of the nanobodies and a maleimide-PEG linker on the nanoparticles. To test whether random SATA modifications would affect the integrity of the selected nanobodies, different amounts of SATA were allowed to react with C3, F5 and G2 and the effect of these modifications on binding affinity was studied on MKN45 cells (Fig. S2A-C). The introduction of SATA moieties to C3 and F5 did decrease their binding affinity to MKN45 cells by two fold, whereas G2, even with high modification ratios, was not affected (K_D of ~1 nM for all degrees of modification). The degree of SATA modification in G2, the average amount of SATA modifications per molecule, was quantified by capillary electrophoresis followed by time-of-flight mass spectrometry (CE-TOF-MS) (Fig. 2A). The molecular weight found for peak 1 (17.6 kDa) corresponded to the unconjugated G2 nanobody. The subsequent increases in molecular weight (peak 2–6) corresponded well with the calculated mass of the introduced SATA groups (116 Da). G2 carrying 1 to 4 SATA modifications accounted for more than 90% of the relative peak area and on average, a conjugation of approximately 2.4 SATA molecules per G2 nanobody was found.

3.3. Preparation and characterization of G2-coupled albumin nanoparticles

The SATA-modified G2 nanobody was coupled to the PEGylated nanoparticles (NP) to generate G2 decorated nanoparticles (G2-PEG-NP). The coupling efficiency of SATA-modified G2 to albumin nanoparticles was investigated by reacting increasing amounts of G2 with the PEGylated nanoparticles, followed by dot-blot analysis of the nanoparticles with anti-VHH antiserum. Nanobody coupling was found to be saturated at G2:NP ratios of 6 nmol/mg NP and higher (Fig. 2B). The covalent attachment of G2 to the PEG anchor was confirmed by SDS-PAGE analysis of G2-PEG-NP, which showed the absence of unbound G2, indicating complete binding of G2 nanobodies to the nanoparticles (data not shown). Size determination of the nanoparticles showed that the G2-decorated nanoparticles were approximately 100 nm in size after PEGylation (polydispersity <0.1) and had a slightly negative zeta potential of −19 mV (Table 1).

3.4. The anti-met NANAPs bind specifically to Met-expressing cells

The specificity of the G2-coupled nanoparticles was determined by studying the binding of IRDye800-conjugated PEG-NP and G2-PEG-NP to either Met-negative TOV-112D cells or the TOV + Met variant (Fig. 3A–B, left). Both non-targeted PEG-NP and targeted G2-PEG-NP showed some binding to the Met-negative cells. The linear fashion in which this binding was detected was considered to be indicative of non-specific low-affinity interactions. Importantly, G2-PEG-NP showed specific binding to TOV + Met cells with a half-maximal binding of approximately 0.15 mg/ml. Fluorescence microscopy imaging with Alexa488-labeled nanoparticles confirmed specific binding of G2-PEG-NP to TOV + Met cells and low background binding to Met-negative cells (Fig. 3A–B, right). Similar results with respect to binding specificity were obtained with the Met-expressing tumor cell lines, A549 and MKN45. Only G2-PEG-

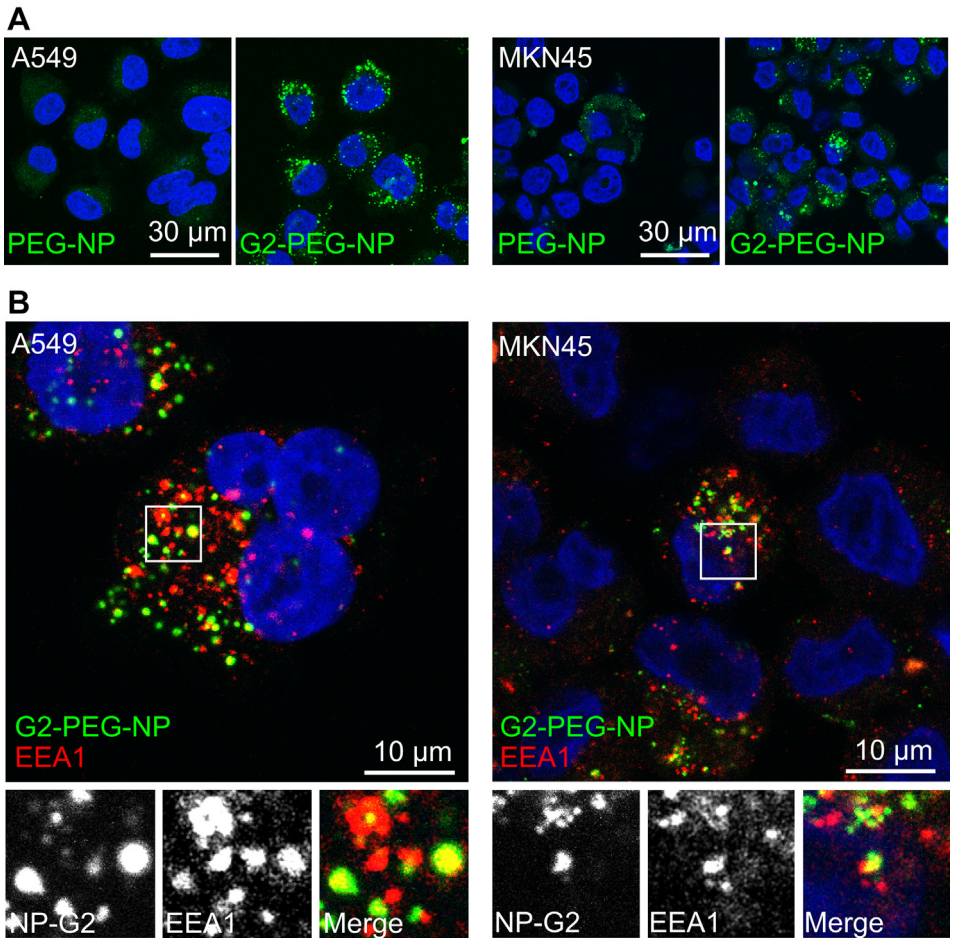

Fig. 5. G2-PEG-NP internalize specifically into Met-expressing cells. A) A549 (left) and MKN45 (right) cells were incubated with Alexa488-conugated G2-PEG-NP or PEG-NP for 2 h at 37 °C. B) Cells were incubated as in A and subsequently fixated and permeabilized. Early endosomes were stained with anti-EEA1 antibodies and nuclei were stained with DAPI (blue).

NP showed membrane binding to the Met-expressing tumor cell lines while untargeted PEG-NP showed only low (background) binding (Fig. 3C–D).

3.5. NANAPs induce Met phosphorylation but no cell scattering

In order to study whether the observed nanoparticle uptake is accompanied by receptor activation, their agonistic/antagonistic properties were determined on A549 cells by western blotting (Fig. 4A). The G2 nanobody alone did not stimulate Met activity at a low concentration (1 nM), but at higher concentration (1 μM) the Met receptor was clearly phosphorylated. As expected, PEG-NP did not result in Met activation, but the targeted G2-PEG-NP stimulated Met activity at all concentrations tested (Fig. 4A, left). To test whether the nanobodies or nanoparticles would have an intrinsic therapeutic activity by blocking ligand binding, A549 cells were incubated with G2 or nanoparticles, in the presence and absence of HGF. None of the formulations blocked HGF-induced phosphorylation of Met (Fig. 4A, right). Also in the MKN45 cells, none of the formulations were able to reduce receptor activation of Met (Fig. S3). To investigate whether the agonistic property of G2-PEG-NP as observed by Met activation would have an actual downstream effect, we performed a scratch wound assay (Fig. 4B, left). For this experiment, A549 cells were used, since the constitutive activation of Met in MKN45 cells make them non-responsive to the ligand for Met. G2, PEG-NP or G2-PEG-NP did not induce wound closure, a complete closure of the scratch wound was only observed upon treatment with HGF. This means that, even though the G2-PEG-NP or G2 (only at 1 μM) are able to cause phosphorylation of Met, this is insufficient to induce cell scattering of A549 cells. A similar approach was chosen to investigate the downstream antagonistic effect of the anti-Met nanobodies or nanoparticles (Fig. 4B, right). Here, the wound closing effect of HGF was partially blocked by a high concentration of G2 and by the G2-PEG-NPs. Despite inducing Met phosphorylation, the anti-Met NANAPs do inhibit cell scattering and thereby wound healing in A549 cells.

3.6. Internalization, lysosomal sorting and degradation of Met and G2-PEG-NP

Eventually, anti-Met NANAPs could function as a nanocarrier for the intracellular delivery of therapeutic agents. We therefore assessed whether the G2-PEG-NPs were internalized by Met-expressing cells using confocal fluorescence microscopy. After 2 h of incubation, specific uptake of only the G2-PEG-NP could be observed in both A549 and MKN45 cells, as indicated by an intracellular endosomal staining pattern (Fig. 5A). Co-staining of the cells with early endosomal marker EEA-1 showed that the internalized nanoparticles were localized in early endosomes, which is apparent from the yellow color in the merged image with green-labeled nanoparticles and red-labeled-EEA-1 (Fig. 5B). Nevertheless, not all G2-PEG-NP were located in early endosomes at this

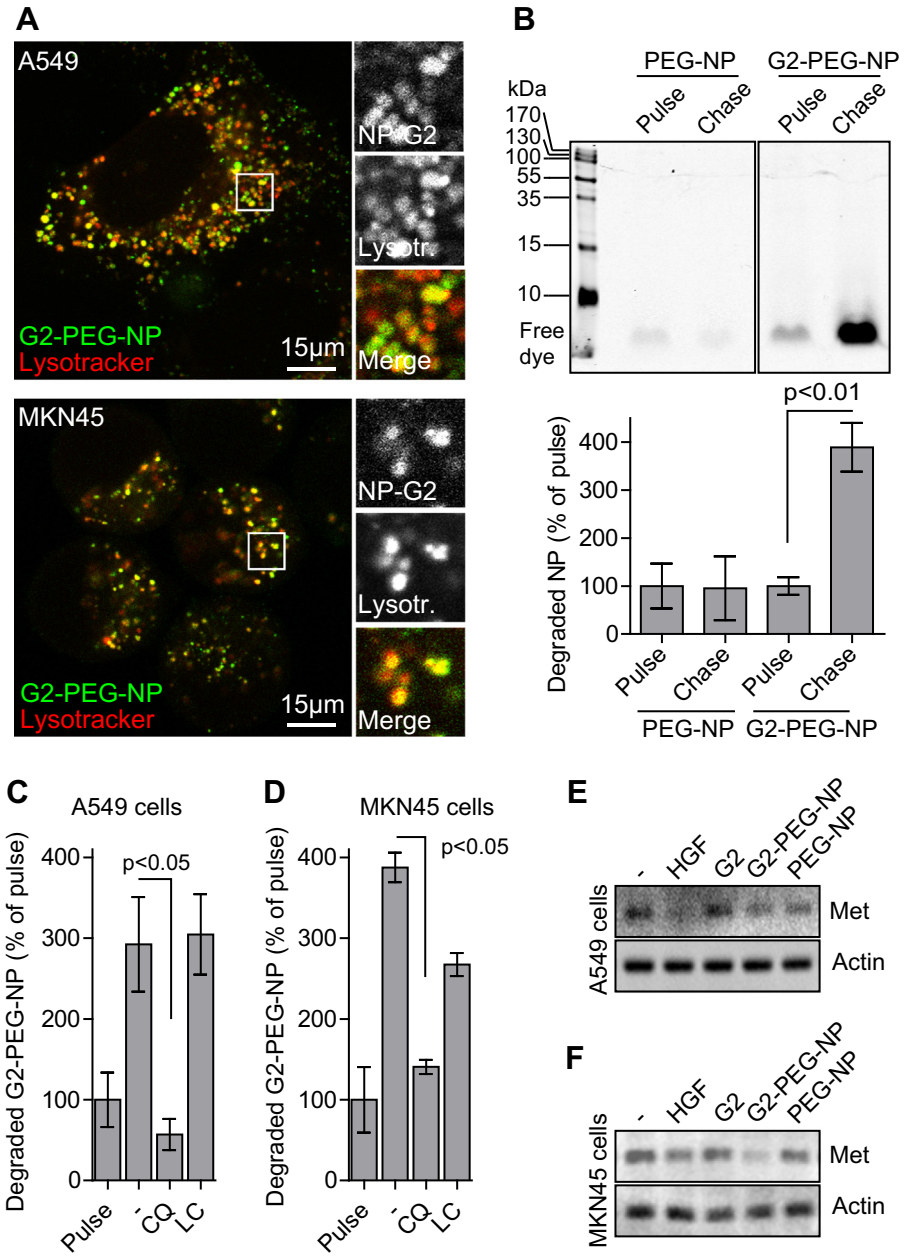

Fig. 6. Anti-Met NANAPs are degraded by lysosomes and induce receptor downregulation. A) A549 (top) and MKN45 (bottom) cells were incubated with Alexa488-conjugated G2-PEG-NP for 16 h and fixed for confocal fluorescence imaging. Late endosomes and lysosomes were stained with Lysotracker-Red. B) MKN45 cells were pulsed for 2 h with IRDye800-conjugated PEG-NP or G2-PEG-NP and chased for 16 h. Cells were lysed and free dye was separated from intact nanoparticles by electrophoresis. Degradation of G2-PEG-NP is apparent as the appearance of free dye (green) at the bottom of the gel and was quantified using the Odyssey Infrared scanner (right panel). C) A549 cells or D) MKN45 cells were incubated with IRDye800-conjugated G2-PEG-NP in the absence or presence of the inhibitors chloroquine (CQ) and Lactacystin (LC) after which the appearance of free dye was quantified as in B. E, F) Met downregulation 48 h after treatment with HGF (50 ng/ml), G2 (100 nM), PEG-NP (0.5 mg/ml) and G2-PEG-NP (0.5 mg/ml) on E) A549 and F) MKN45 cells. Error bars represent SEM where $n = 3$.

time point, which could be due to the highly dynamic nature of endocytic vesicles, in which cargo is rapidly transported to further downstream compartments like sorting and late endosomes and eventually lysosomes [30].

To investigate whether the nanoparticles were routed towards late endosomes or lysosomes, co-localization of Alexa488-labeled G2-PEG-NP with Lysotracker Red was studied in A549 and MKN45 cells by confocal fluorescence microscopy (Fig. 6A). After 16 h of incubation, the G2-PEG-NP co-localized almost completely with lysotracker Red, indicating that these NANAPs indeed end up in late-endosomal/lysosomal compartments. To check whether the nanoparticles were also degraded, a pulse-chase experiment was performed with IRDye800-labeled G2-PEG-NP or PEG-NP. After 16 h, degradation of the nanoparticles was observed by SDS-PAGE, which is apparent by the appearance of free IRDye800 at the bottom of the gel (Fig. 6B). Only Met-targeted nanoparticles showed signs of degradation, which is in good correlation with the specific binding and internalization of the G2-PEG-NP mentioned above (Fig. 5A).

In general, protein degradation in cells is mediated by the proteasome complex and/or by the proteases in the endosomal/lysosomal system. Lysosomal degradation of Met plays an important role in the ligand-induced negative feedback mechanism of Met [15]. In addition, it has been reported that ligand-induced

degradation of Met is also regulated by proteasomal degradation [31]. To study the nature of the observed degradation of the nanoparticles in more detail, we inhibited both lysosomal and proteasomal degradation with either the lysosome inhibitor chloroquine (CQ), and the proteasome inhibitor lactacystin (LC). In both A549 and MKN45 cells, co-incubation with 10 μM of CQ for 16 h blocked the degradation of the G2-PEG-NP almost completely (Fig. 6C–D). In contrast, LC had no effect on nanoparticle degradation in A549 cells and a minor effect in MKN45 cells.

This lysosomal targeting makes the anti-Met NANAPs suitable for the intracellular delivery and release of therapeutic compounds. In addition, lysosomal trafficking of Met induced by the NANAPs could potentially lead to receptor downregulation in Met-overexpressing tumors. This is particularly interesting for tumors that highly overexpress Met and thereby induce constitutive activation of the receptor, as is the case with the MKN45 cell line (Fig. S3). To investigate whether lysosomal degradation of G2-PEG-NP is accompanied by receptor degradation, cells were incubated with G2, PEG-NP, G2-PEG-NP and HGF for 48 h after which total Met protein levels were determined by western blotting (Fig. 6E–F). While HGF most prominently induced Met downregulation in A549 cells, treatment with G2-PEG-NP down regulated total Met protein in both A549 and MKN45 cells. All together, these data indicate that anti-Met NANAPs are primarily translocated to late endosomes and lysosomes, which eventually results in lysosomal degradation of both the nanoparticles and Met receptors.

4. Discussion

Met overexpression is correlated with poor prognosis in most of the aggressive cancers, such as brain, liver, pancreatic cancers and gastric carcinoma [8]. Targeted delivery of small-molecule drugs can contribute to selective inhibition or even killing of Met-expressing tumor cells. In this study, we performed phage display selections for nanobodies specifically binding to human Met, and evaluated the applicability of an anti-Met nanobody for targeting albumin nanoparticles to Met-expressing tumor cells. Several anti-Met nanobodies were obtained that were specifically binding to Met with high affinity. Besides binding Met, the selected nanobodies could compete for HGF binding to recombinant Met ectodomain. However, this competition was not observed on cells. Although the contrast between these observations is quite evident, it might be explained by a mechanistic difference between binding of HGF to isolated and cellular Met. HGF binding to Met occurs via two interaction sites, the SEMA domain and the immunoglobulin-like region of Met [37,38]. Binding of HGF to the SEMA domain is considered to induce a conformational change of the ectodomain, revealing the second binding position on the Ig-like regions. Possibly, the interaction of the radiolabeled HGF and the coated recombinant ectodomain only involves one of these binding domains and therefore the binding of HGF could easily be disrupted by the selected nanobodies. Moreover, the binding of HGF to Met on cells is considered to be further stabilized by secondary interactions of HGF with heparin sulphate, which is present on the plasma membrane [28]. The fact that G2-PEG-NPs did not compete with HGF on cells also suggest that the potential therapeutic effects of the NANAP's *in vivo* would be independent of HGF levels.

The anti-Met nanobody was efficiently conjugated to the albumin nanoparticles, which allowed their specific binding to Met-expressing tumor cells. A disadvantage of the nanobody is the possible effect of the conjugation of a chemical compound as SATA on the affinity. This is especially the case when the site of interaction is located in one of the CDR regions of the nanobody. We have recently shown that by introducing an additional cysteine at the C-terminus of a nanobody and using this for site-directed conjugation, effects on binding affinity can be avoided [36]. Here, the effect of SATA modification on the binding affinity of the selected anti-Met nanobodies was tested and revealed only a small effect for only one of the nanobodies. This indicates that the SATA groups probably do not bind to a lysine present in the antigen-binding region.

Previously, similar nanoparticles were used to retarget toxins like doxorubicin and fluorescent dyes like Cy5 using whole antibodies or peptides directed against avβ3-integrins, the chemokine receptor 4 (CXCR4), or somatostatin receptors [32–34]. Recently, Lu et al. reported the selection of anti-Met single chain antibodies (scFv) that were used for targeting of quantum dots or doxorubicin loaded liposomes [35]. The affinity of the reported scFv's was studied on isolated Met and was about 10-fold less than our anti-Met nanobodies, which were tested on Met-positive cells. The affinity of the G2-nanobody was in the low nanomolar range, which explains the efficient binding of the G2-PEG-NP to the Met-expressing cells.

The agonistic activity of G2-PEG-NP is possibly induced by receptor clustering via the multivalent anti-Met format of the nanoparticles. The fact that this was insufficient to induce cell migration, suggests that the NANAPs were unable to fully activate all downstream pathways of Met towards migration. Similar differential downstream signaling towards cell motility, invasion and proliferation was observed with different agonistic antibodies against Met [39]. Possibly, the nanoparticles and antibodies induce only a minor activation of Met, which is insufficient to activate downstream pathways. A recent study with oral squamous carcinoma cells showed that, despite a clear phosphorylation of Met, scratch wound healing occurred dose-dependently and only above a certain threshold concentration of HGF (no wound healing at 3.7 ng/ml of HGF to a clear healing at 33 ng/ml) [40]. These data suggest the existence of a threshold of Met activation requires for the full range of biological responses. Since Met activation by either G2 or G2-PEG-NP did not result in a cellular response like cell migration, we consider their agonistic properties to be of little consequence for future use of the nanoparticles.

In general, the internalization of drug loaded and targeted nanocarriers greatly enhances the specific killing of the targeted cells [12,41,42]. The efficacy of antibodies or nanoparticles can be enhanced by employing receptor-mediated uptake. We have previously shown that internalizing liposomes decorated with anti-EGFR nanobodies reduced total EGFR protein expression and inhibited cell growth more potently than a nanobody alone [19]. The nanoparticles in this study also internalized and were subsequently targeted to lysosomes where they were degraded. Internalization of these complexes might be initiated by complex formation of Met as previously suggested by the induced internalization of EGFR using anti-EGFR nanobodies bound to liposomes [19]. The anti-EGFR liposomes did not stimulate tyrosine kinase activity of EGFR, which is in contrast to the G2-PEG-NPs. While this activation did not result in cell scattering, it resulted in Met receptor and eventually downregulation. This reduces the overactivation of this pathway, which could potentially contribute to the inhibition of tumor growth as we previously have shown for the EGFR [19]. In a study by Petrelli et al., Met downregulation was shown to reduce tumor size regardless of receptor phosphorylation [43]. As such, the G2-PEG-NP could therefore have an intrinsic anti-tumor activity, as observed in the scratch wound assay (Fig. S2), where G2-PEG-NPs inhibited wound healing in A549 cells.

5. Conclusion

We have generated nanobodies specifically binding to Met, which were used to target human albumin nanoparticles to Met-expressing cells. The anti-Met NANAPs are internalized by Met-

expressing cells and transported to lysosomes for degradation of both NANAPs and receptor. We conclude that the nanoparticles as designed and characterized in this paper are a good candidate for the selective delivery of chemotherapeutic drugs in the treatment of Met overexpressing tumors.

Acknowledgements

This study was funded by the Focus & Massa project of the Utrecht University, The Netherlands

Appendix A. Supplementary data

Supplementary data related to this article can be found at http://dx.doi.org/10.1016/j.biomaterials.2013.10.001.

References

[1] Naldini L, Vigna E, Narsimhan RP, Gaudino G, Zarnegar R, Michalopoulos GK, et al. Hepatocyte growth factor (HGF) stimulates the tyrosine kinase activity of the receptor encoded by the proto-oncogene c-MET. Oncogene 1991;6(4):501–4.
[2] Ferracini R, Longati P, Naldini L, Vigna E, Comoglio PM. Identification of the major autophosphorylation site of the Met/hepatocyte growth factor receptor tyrosine kinase. J Biol Chem 1991;266(29):19558–64.
[3] Bussolino F, Di Renzo MF, Ziche M, Bocchietto E, Olivero M, Naldini L, et al. Hepatocyte growth factor is a potent angiogenic factor which stimulates endothelial cell motility and growth. J Cell Biol 1992;119(3):629–41.
[4] Xiao GH, Jeffers M, Bellacosa A, Mitsuuchi Y, Vande Woude GF, Testa JR. Anti-apoptotic signaling by hepatocyte growth factor/Met via the phosphatidylinositol 3-kinase/Akt and mitogen-activated protein kinase pathways. Proc Natl Acad Sci U S A 2001;98(1):247–52.
[5] Birchmeier C, Gherardi E. Developmental roles of HGF/SF and its receptor, the c-Met tyrosine kinase. Trends Cell Biol 1998;8(10):404–10.
[6] Chmielowiec J, Borowiak M, Morkel M, Stradal T, Munz B, Werner S, et al. c-Met is essential for wound healing in the skin. J Cell Biol 2007;177(1):151–62.
[7] Huh CG, Factor VM, Sanchez A, Uchida K, Conner EA, Thorgeirsson SS. Hepatocyte growth factor/c-met signaling pathway is required for efficient liver regeneration and repair. Proc Natl Acad Sci U S A 2004;101(13):4477–82.
[8] Birchmeier C, Birchmeier W, Gherardi E, Vande Woude GF. Met, metastasis, motility and more. Nat Rev Mol Cell Biol 2003;12:915–25.
[9] Corso S, Comoglio PM, Giordano S. Cancer therapy: can the challenge be MET? Trends Mol Med 2005;11(6):284–92.
[10] Knudsen BS, Vande Woude G. Showering c-MET-dependent cancers with drugs. Curr Opin Genet Dev 2008;18(1):87–96.
[11] Liu X, Newton RC, Scherle PA. Developing c-MET pathway inhibitors for cancer therapy: progress and challenges. Trends Mol Med 2010;16(1):37–45.
[12] Iyer U, Kadambi VJ. Antibody drug conjugates - Trojan horses in the war on cancer. J Pharmacol Toxicol Methods 2011;64(3):207–12.
[13] Li N, Hill KS, Elferink LA. Analysis of receptor tyrosine kinase internalization using flow cytometry Methods Mol Biol;457:305–317.
[14] Eierhoff T, Hrincius ER, Rescher U, Ludwig S, Ehrhardt C. The epidermal growth factor receptor (EGFR) promotes uptake of influenza A viruses (IAV) into host cells. PLoS Pathog 2010;6(9):e1001099.
[15] Lefebvre J, Ancot F, Leroy C, Muharram G, Lemiere A, Tulasne D. Met degradation: more than one stone to shoot a receptor down. FASEB J 2012;26(4):1387–99.
[16] Altintas I, Heukers R, van der Meel R, Lacombe M, Amidi M, van Bergen En Henegouwen PM, et al. Nanobody-albumin nanoparticles (NANAPs) for the delivery of a multikinase inhibitor 17864 to EGFR overexpressing tumor cells. J Control Release 2013;165(2):110–8.
[17] Hamers-Casterman C, Atarhouch T, Muyldermans S, Robinson G, Hamers C, Songa EB, et al. Naturally occurring antibodies devoid of light chains. Nature 1993;363(6428):446–8.
[18] Altintas I, Kok RJ, Schiffelers RM. Targeting epidermal growth factor receptor in tumors: from conventional monoclonal antibodies via heavy chain-only antibodies to nanobodies. Eur J Pharm Sci 2012;45(4):399–407.
[19] Oliveira S, Schiffelers RM, van der Veeken J, van der Meel R, Vongpromek R, van Bergen En Henegouwen PM, et al. Downregulation of EGFR by a novel multivalent nanobody-liposome platform. J Control Release 2010;145(2):165–75.
[20] Talelli M, Oliveira S, Rijcken CJ, Pieters EH, Etrych T, Ulbrich K, et al. Intrinsically active nanobody-modified polymeric micelles for tumor-targeted combination therapy. Biomaterials 2013;34(4):1255–60.
[21] Hofman EG, Ruonala MO, Bader AN, van den Heuvel D, Voortman J, Roovers RC, et al. EGF induces coalescence of different lipid rafts. J Cell Sci 2008;121(Pt 15):2519–28.
[22] Salacinski PR, McLean C, Sykes JE, Clement-Jones VV, Lowry PJ. Iodination of proteins, glycoproteins, and peptides using a solid-phase oxidizing agent, 1,3,4,6-tetrachloro-3 alpha,6 alpha-diphenyl glycoluril (Iodogen). Anal Biochem 1981;117(1):136–46.
[23] Langer K, Balthasar S, Vogel V, Dinauer N, von Briesen H, Schubert D. Optimization of the preparation process for human serum albumin (HSA) nanoparticles. Int J Pharm 2003;257(1–2):169–80.
[24] Haselberg R, de Jong GJ, Somsen GW. Capillary electrophoresis of intact basic proteins using noncovalently triple-layer coated capillaries. J Sep Sci 2009;32(14):2408–15.
[25] Haselberg R, de Jong GJ, Somsen GW. Capillary electrophoresis-mass spectrometry of intact basic proteins using polybrene-dextran sulfate-Polybrene-coated capillaries: system optimization and performance. Anal Chim Acta 2010;678(1):128–34.
[26] Haselberg R, Brinks V, Hawe A, de Jong GJ, Somsen GW. Capillary electrophoresis-mass spectrometry using noncovalently coated capillaries for the analysis of biopharmaceuticals. Anal Bioanal Chem 2011;400(1):295–303.
[27] Liang CC, Park AY, Guan JL. In vitro scratch assay: a convenient and inexpensive method for analysis of cell migration in vitro. Nat Protoc 2007;2(2):329–33.
[28] Lyon M, Deakin JA, Mizuno K, Nakamura T, Gallagher JT. Interaction of hepatocyte growth factor with heparan sulfate. Elucidation of the major heparan sulfate structural determinants. J Biol Chem 1994;269(15):11216–23.
[29] Frenken LG, van der Linden RH, Hermans PW, Bos JW, Ruuls RC, de Geus B, et al. Isolation of antigen specific llama VHH antibody fragments and their high level secretion by *Saccharomyces cerevisiae*. J Biotechnol 2000;78(1):11–21.
[30] Gruenberg J. The endocytic pathway: a mosaic of domains. Nat Rev Mol Cell Biol 2001;2(10):721–30.
[31] Hammond DE, Urbe S, Vande Woude GF, Clague MJ. Down-regulation of MET, the receptor for hepatocyte growth factor. Oncogene 2001;20(22):2761–70.
[32] Wagner S, Rothweiler F, Anhorn MG, Sauer D, Riemann I, Weiss EC, et al. Enhanced drug targeting by attachment of an anti alphav integrin antibody to doxorubicin loaded human serum albumin nanoparticles. Biomaterials 2010;31(8):2388–98.
[33] Bunschoten A, Buckle T, Kuil J, Luker GD, Luker KE, Nieweg OE, et al. Targeted non-covalent self-assembled nanoparticles based on human serum albumin. Biomaterials 2012;33(3):867–75.
[34] Bae S, Ma K, Kim TH, Lee ES, Oh KT, Park ES, et al. Doxorubicin-loaded human serum albumin nanoparticles surface-modified with TNF-related apoptosis-inducing ligand and transferrin for targeting multiple tumor types. Biomaterials 2012;33(5):1536–46.
[35] Lu RM, Chang YL, Chen MS, Wu HC. Single chain anti-c-Met antibody conjugated nanoparticles for in vivo tumor-targeted imaging and drug delivery. Biomaterials 2011;32(12):3265–74.
[36] Kijanka M, Warnders FJ, El Khattabi M, Lub-de Hooge M, van Dam GM, Ntziachristos V, et al. Rapid optical imaging of human breast tumour xenografts using anti-HER2 VHHs site-directly conjugated to IRDye 800CW for image-guided surgery Eur J Nucl Med Mol Imaging 2013;40(11):1718–29.
[37] Stamos J, Lazarus RA, Yao X, Kirchhofer D, Wiesmann C. Crystal structure of the HGF beta-chain in complex with the Sema domain of the Met receptor. EMBO J 2004;23(12):2325–35.
[38] Basilico C, Arnesano A, Galluzzo M, Comoglio PM, Michieli P. A high affinity hepatocyte growth factor-binding site in the immunoglobulin-like region of Met. J Biol Chem 2008;283(30):21267–77.
[39] Prat M, Crepaldi T, Pennacchietti S, Bussolino F, Comoglio PM. Agonistic monoclonal antibodies against the Met receptor dissect the biological responses to HGF. J Cell Sci 1998;111(Pt 2):237–47.
[40] Brusevold IJ, Aasrum M, Bryne M, Christoffersen T. Migration induced by epidermal and hepatocyte growth factors in oral squamous carcinoma cells in vitro: role of MEK/ERK, p38 and PI-3 kinase/Akt. J Oral Pathol Med 2012;41(7):547–58.
[41] Sapra P, Allen TM. Internalizing antibodies are necessary for improved therapeutic efficacy of antibody-targeted liposomal drugs. Cancer Res 2002;62(24):7190–4.
[42] Bai F, Wang C, Lu Q, Zhao M, Ban FQ, Yu DH, et al. Nanoparticle-mediated drug delivery to tumor neovasculature to combat P-gp expressing multidrug resistant cancer. Biomaterials 2013;34(26):6163–74.
[43] Petrelli A, Circosta P, Granziero L, Mazzone M, Pisacane A, Fenoglio S, et al. Ab-induced ectodomain shedding mediates hepatocyte growth factor receptor down-regulation and hampers biological activity. Proc Natl Acad Sci U S A 2006;103(13):5090–5.